# Tetrahedral coordination and low-spin configuration in a 5*d* oxide

Q. Zhao,[1] J.-H. Sim,[2] Z. Zhang,[3] H. Su,[4] F. Han,[5] Q. Zhang,[6] B. Tian,[1] Q. Xu,[7] M.-J. Han,[2,*] C.-G. Duan,[1,†] and J. F. Mitchell[5]

[1]*Key Laboratory of Polar Materials and Devices (MOE), Department of Optoelectronics, East China Normal University, Shanghai 200241, China*

[2]*Department of Physics, KAIST Daejeon 305-701, Korea*

[3]*Pharmaceutical Analytical & Solid-State Chemistry Research Center, Shanghai Institute of Materia Medica, Chinese Academy of Sciences, Shanghai 201203, China*

[4]*Chongqing Institute of Green and Intelligent Technology, Chinese Academy of Sciences, Chongqing 400714, China*

[5]*Material Science Division, Argonne National Laboratory, Lemont, Illinois 60439, USA*

[6]*Department of Chemistry, Washington State University, Pullman, Washington 99164, USA*

[7]*New Energy Research Institute, China University of Petroleum, Beijing 102200, China*

(Received 19 December 2018; revised manuscript received 7 March 2019; published 17 June 2019)

Spin state plays a key role in a plethora of physical, biological, and geological phenomena. In octahedral coordination, spin state of 3*d* transition metals can be high spin or low spin, and can be tuned with external stimuli. In a tetrahedral coordination environment, with the smaller crystal field splitting energy, only high spin is considered possible for oxides. Herein we report the realization of low spin state in tetrahedral coordination in a novel oxide, $Sr_9Ir_3O_{17}$. The low spin configuration was confirmed with density functional theory (DFT) calculations, including the effect of spin-orbit coupling (SOC), electron-electron repulsion ($U$), magnetic data, and crystal chemical consideration. This exotic electronic configuration was realized with the confluence of extended 5*d* orbitals, short bond lengths, and an electron count maximizing the crystal field stabilization energy. The discovery of low spin state for a tetrahedral environment provides a novel platform for spin state manipulation in solid state materials.

DOI: 10.1103/PhysRevMaterials.3.063607

## I. INTRODUCTION

Spin state plays an essential role in a plethora of geological, biological, and physical phenomena. For instance, the spin-state transition in magnesiowüstite was found to be linked to the seismic-wave heterogeneity in the Earth's lower mantle [1]. In biology, the spin state of Fe plays an important role in the cooperative release of oxygen from oxyhemoglobin [2]. For molecular complexes, supramolecular systems, and coordination polymers, spin crossover phenomena have attracted intense interests [3]. For oxides, spin state transition is related to many important physical phenomena, for instance, charge ordering [4], metal-insulator transitions [5], and magnetoresistance [6].

While for octahedral coordination the manipulation of spin state has been shown in many oxides, for tetrahedral coordination only high spin state is known in oxides and low spin state has not been reported. Since 5*d* orbitals offer the extended characteristics allowing for stronger overlapping, we seek to 5*d* transition metal oxides for realizing exotic low spin states in tetrahedral coordination. However, only several 5*d* transition metal oxides are known to have tetrahedral coordination, and they are all limited to either $d^0$ and $d^1$ configuration [7–9], for which spin state is apparently irrelevant.

Iridium, with a $6s^25d$ [7] electron configuration, is known to have various high oxidation states [10]. Herein we demonstrate that an exotic low spin state in tetrahedral coordination is realized in a novel iridate $Sr_9Ir_3O_{17}$. First-principles electronic structure calculations calculation within generalized gradient approximation and including spin-orbit coupling and electron-electron repulsion (GGA+SOC+$U$) and magnetic data consistently demonstrate that the Ir cation in the tetrahedron adopts a low spin $S = 0$ state as its ground state configuration. The low spin configuration is further corroborated with the unusually short bond lengths. The discovery of low spin state on tetrahedral sites can provide a novel platform for spin state manipulation.

## II. EXPERIMENTAL METHODS

### A. Synthesis

$Sr_9Ir_3O_{17}$ crystals were synthesized via two methods. For method 1, Ir metal (0.8 mmol), $SrCO_3$ (1 g, 6.8 mmol), and $K_2CO_3$ (5 g, 36.2 mmol) were loaded into a 10 ml alumina crucible with lid. The crucible was placed into a box furnace, heated to 1050 °C at 300 °C/h, held at that temperature for 12 h, cooled to 900 °C at 5 °C/h, and finally cooled to room temperature by turning off the furnace. For method 2, Ir metal (2 mmol), $SrCO_3$ (1 g, 6.8 mmol), and $K_2CO_3$ (5 g, 36.2 mmol) were loaded into a 10 ml alumina crucible with lid. The crucible was placed into a tube furnace with oxygen flow, heated to 1050 °C at 300 °C/h, held at that temperature

*Corresponding author: mj.han@kaist.ac.kr
†Corresponding author: cgduan@clpm.ecnu.edu.cn

 

TABLE I. Crystal data and structure refinement for $Sr_9Ir_3O_{17}$.

| | |
|---|---|
| Empirical formula | $Sr_9Ir_3O_{17}$ |
| Formula weight | 1637.16 |
| Temperature | 100 K |
| Wavelength | 0.71073 Å |
| Crystal system | Monoclinic |
| Space group | *C*2/*c* |
| Unit cell dimensions | $a = 28.493(6)$ Å, $\alpha = 90.00^\circ$<br>$b = 11.876(2)$ Å, $\beta = 93.33(3)^\circ$<br>$c = 9.969(2)$ Å, $\gamma = 90.00^\circ$ |
| Volume | 3367.7(12) Å$^3$ |
| Z | 8 |
| Density (calculated) | 6.458 g/cm$^3$ |
| Absorption coefficient | 51.941 mm$^{-1}$ |
| *F*(000) | 5672 |
| $\theta$ range for data collection | 1.43° to 25.00° |
| Index ranges | $-33 \Leftarrow h \Leftarrow 33$, $-14 \Leftarrow k \Leftarrow 14$, $-11 \Leftarrow l \Leftarrow 11$ |
| Reflections collected | 26 652 |
| Independent reflections | 2967[$R_{\text{int}} = 0.073$] |
| Completeness to $\theta = 25.00^\circ$ | 100% |
| Refinement method | Full-matrix least-squares on $F^2$ |
| Data / restraints / parameters | 2972 / 18 / 263 |
| Goodness-of-fit | 1.035 |
| Final *R* indices [$>2\sigma(I)$][a] | $R_{\text{obs}} = 0.0446$, $wR_{\text{obs}} = 0.1099$ |
| *R* indices [all data] | $R_{\text{all}} = 0.0654$, $wR_{\text{all}} = 0.1208$ |
| Largest diff. peak and hole | 3.86 and $-5.06\,e$ Å$^{-3}$ |

[a]$R = \Sigma||F_o|-|F_c||/\Sigma|F_o|$, $wR = \{\Sigma[w(|F_o|^2 - |F_c|^2)^2]/\Sigma[w(|F_o|^4)]\}^{1/2}$ and calc $w = 1/[\sigma^2(Fo^2) + (0.0231P)^2 + 330.6570P]$, where $P = (Fo^2 + 2Fc^2)/3$.

for 12 h, cooled to 900 °C at 5 °C/h, and finally cooled to room temperature by turning off the furnace. For both methods, the crystals were separated by dissolving the flux in water aided by sonication, and then isolated by vacuum filtration and rinsing with acetone. The slightly air-sensitive crystals were stored in a glovebox prior to measurements.

It was noted that by method 1 (crystal growth in air), the crystal growth seems to be affected by humidity. In a rather dry atmosphere, pure samples of $Sr_9Ir_3O_{17}$ can be synthesized with good crystal quality suitable for single crystal x-ray diffraction. However, in a more humid atmosphere, crystals of $Sr_9Ir_3O_{17}$ are accompanied by competing phases like $Sr_2IrO_4$ and/or $Sr_4IrO_6$. This possibly arises from a reaction of high valent Ir in the flux with $H_2O$ in air, which partially converts it into $Ir^{4+}$. Ir in various oxidation states (0, +4, and undetermined oxidation states) is well known to have oxygen evolution reaction (OER) activities [11,12]. Although the detailed report of OER activity for high valent Ir is lacking, it is likely that high valent Ir can have a stronger tendency to gain electrons, and in this case, from $H_2O$ in humid air. In method 2, with $O_2$ flow, pure samples of $Sr_9Ir_3O_{17}$ can be consistently synthesized in nearly 100% purity, likely due to the elimination of $H_2O$. However, the crystal quality (as adjudged by x-ray diffraction) obtained by method 1 is better than method 2.

### B. Single crystal x-ray diffraction and crystal structure

Single crystals grown by method 1 were selected and affixed to the tips of glass fibers and then mounted on a Bruker APEX II 3-circle diffractometer equipped with an APEX II detector. Data collection was carried out at 100 K using Mo $K_\alpha$ radiation ($\lambda = 0.71073$ Å) with a detector distance of 5.00 cm. Five major sections of frames were collected with 0.50°$\varphi$ and $\omega$ scans. Data to a resolution of 0.84 Å were considered in the reduction. The raw intensity data were corrected for absorption (SADABS). The crystal structure was solved with the SHELXT software package via the direct method, and refined by full-matrix least-square techniques [13]. The parameters for data collection and the details of the structure refinement are given in Table I. Atomic coordinates are shown in Table II. The anisotropic thermal parameters are shown in Appendix A.

### C. X-ray absorption near edge spectroscopy (XANES)

X-ray absorption near edge spectroscopy (XANES) experiments were carried out at the Sector 20-bending magnet beamline in the Advanced Photon Source at Argonne National Laboratory. The samples were ground into fine powders, and mixed thoroughly with boron nitride and cold pressed into pellets. Samples were measured in a chamber that allows for a continuous helium flow. The measurements were carried out in transmission mode using a Si (111) monochromator. Harmonic contamination was minimized using a rhodium-coated harmonic rejection mirror. An $IrO_2$ pellet was measured periodically to ensure good reproducibility of the x-ray energy. The relative uncertainty in energy between the various samples is estimated to be $\sim\pm0.05$ eV. Data reduction

TABLE II. Atomic coordinates and equivalent isotropic displacement parameters ($Å^2 \times 10^3$) for $Sr_9Ir_3O_{17}$ at 293(2) K with estimated standard deviations in parentheses.

| | $x$ | $y$ | $z$ | $U_{eq}$ [a] |
|---|---|---|---|---|
| Ir1 | 0.66721 (2) | 0.12519 (5) | 0.41527 (5) | 0.0222 (2) |
| Ir2 | 0.5000 | 0.11414 (8) | 0.7500 | 0.0470 (3) |
| Ir3 | 0.5000 | 0.62798 (6) | 0.7500 | 0.0221 (2) |
| Ir4 | 0.66332 (2) | 0.37108 (5) | 0.91139 (5) | 0.0232 (2) |
| Sr1 | 0.72986 (5) | 0.40100 (12) | 0.22627 (14) | 0.0250 (3) |
| Sr2 | 0.54588 (5) | 0.14819 (13) | 0.40318 (14) | 0.0282 (3) |
| Sr3 | 0.57852 (6) | −0.13652 (13) | 0.53097 (15) | 0.0342 (4) |
| Sr4 | 0.59106 (5) | 0.36745 (12) | 0.62468 (14) | 0.0269 (3) |
| Sr5 | 0.71775 (5) | 0.34081 (12) | 0.59007 (13) | 0.0243 (3) |
| Sr6 | 0.64259 (5) | 0.09842 (12) | 0.73466 (13) | 0.0245 (3) |
| Sr7 | 0.53744 (5) | 0.40571 (13) | 0.93390 (14) | 0.0267 (3) |
| Sr8 | 0.61536 (5) | 0.36150 (12) | 1.27705 (14) | 0.0258 (3) |
| Sr9 | 0.79177 (5) | 0.37646 (12) | 0.92087 (16) | 0.0305 (4) |
| O1 | 0.6242 (4) | 0.1265 (8) | 0.2620 (10) | 0.025 (2) |
| O2 | 0.7115 (4) | 0.0371 (9) | 0.3118 (10) | 0.028 (2) |
| O3 | 0.6971 (4) | 0.2637 (8) | 0.3622 (10) | 0.029 (2) |
| O4 | 0.7104 (4) | 0.1231 (8) | 0.5730 (10) | 0.024 (2) |
| O5 | 0.6398 (4) | −0.0153 (8) | 0.4800 (10) | 0.025 (2) |
| O6 | 0.6225 (4) | 0.2138 (9) | 0.5164 (10) | 0.030 (2) |
| O7 | 0.6654 (4) | 0.4477 (9) | 0.7363 (10) | 0.031 (2) |
| O8 | 0.7076 (3) | 0.2536 (9) | 0.8498 (10) | 0.026 (2) |
| O9 | 0.6081 (4) | 0.2767 (8) | 0.8488 (10) | 0.028 (2) |
| O10 | 0.5545 (5) | 0.0451 (13) | 0.7662 (14) | 0.057 (4) |
| O11 | 0.4958 (5) | 0.2213 (12) | 0.8823 (13) | 0.055 (3) |
| O12 | 0.4615 (4) | 0.6270 (8) | 0.5822 (10) | 0.023 (2) |
| O13 | 0.4603 (4) | 0.7449 (9) | 0.8230 (10) | 0.027 (2) |
| O14 | 0.6199 (4) | 0.4860 (9) | 0.9621 (10) | 0.029 (2) |
| O15 | 0.6612 (4) | 0.2999 (8) | 1.0838 (9) | 0.028 (2) |
| O16 | 0.7151 (4) | 0.4621 (8) | 0.9729 (10) | 0.026 (2) |
| O17 | 0.5401 (4) | 0.5100 (8) | 0.6802 (10) | 0.025 (2) |

[a] $U_{eq}$ is defined as one third of the trace of the orthogonalized $U_{ij}$ tensor.

followed standard procedures using the Athena program in the IFEFFIT suite of software [14].

### D. BVS calculations

We attempted to rationalize site-specific oxidation states via a bond valence sum (BVS) approach [15]. BVS parameters for Ir(VI) are lacking, and based on the parameters for Ir(V) [16], the BVS for Ir1, Ir2, Ir3, and Ir4 are 5.49, 5.45, 5.41, and 5.44, respectively. Accordingly, it is impossible to differentiate the oxidation state of these Ir sites solely from BVS.

### E. Density functional theory (DFT) calculations

The first-principles calculations were performed based on density functional theory. All calculations were performed with the software package OpenMX, with the Troullier-Martins-type norm-conserving pseudopotential and the linear combination of pseudoatomic orbitals as a basis set [17,18]. The Perdew-Burke-Ernzerhof (PBE) form of

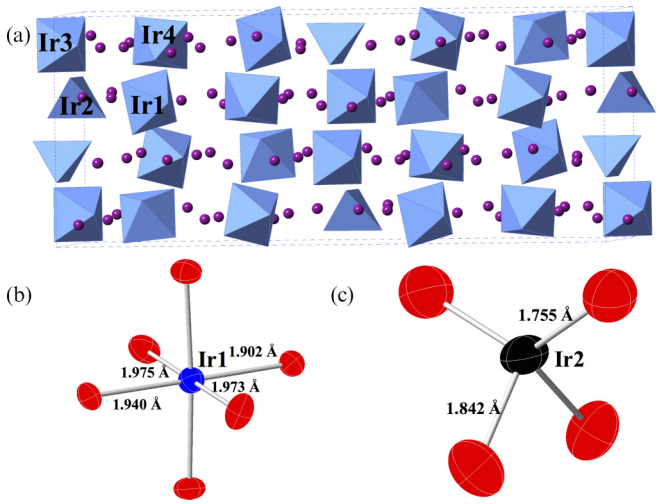


FIG. 1. (a) Crystal structure of $Sr_9Ir_3O_{17}$. $IrO_6$ octahedra and $IrO_4$ tetrahedra are shown in blue, Sr atoms are shown in purple. (b) Representative $IrO_6$ octahedron with the blue ellipsoid representing Ir and red ellipsoids representing O. (c) $IrO_4$ tetrahedron with the black ellipsoid representing Ir and red ellipsoids representing O. In (b) and (c) symmetry unique Ir-O distances are shown.

exchange-correlation functional was adopted [19]. The effect of spin-orbit coupling (SOC) is treated within a fully relativistic $j$-dependent potential in the noncollinear methodology [20]. In order to describe Ir-5$d$ electrons properly, we used GGA+SOC+$U$ formalism (GGA represents for generalized gradient approximations) [21,22] with the effective on-site Coulomb interaction parameter of $U_{eff} = U^{Hubbard} - J^{Hund} =$ 2.0 eV, which is known to be reasonable from the previous studies of iridium oxides (35,36). An energy cutoff of 300 Ry and the Monkhorst-Pack $k$ point mesh of $1\times2\times2$ were used. Our methods and computational details including the numerical parameters have been proved to work well for iridates and other related materials [23–26]. The cluster calculations were carried out by taking $IrO_6$ or $IrO_4$ units directly from the experimental crystal data without structural optimization. In this scheme, the oxidation state and spin configuration of different Ir sites can be simulated by tuning the cluster charge status.

### F. Magnetic property measurements

The dc magnetic susceptibility of the ground samples was measured using a Quantum Design MPMS XL SQUID magnetometer. Samples were measured under zero-field-cooled (ZFC) and field-cooled (FC) conditions in an applied field of 10 kOe. The very small diamagnetic contribution of the gelatin capsule had a negligible contribution to the overall magnetization and was not subtracted.

## III. CRYSTAL STRUCTURE

Single crystals of $Sr_9Ir_3O_{17}$ were synthesized via an oxidizing flux method. The chemical formula and structure were determined by a single-crystal x-ray diffraction method. $Sr_9Ir_3O_{17}$ crystallizes in the monoclinic space group $C2/c$ with the lattice parameters $a = 28.493(6)$ Å,

TABLE III. Selected bond lengths (Å).

| | | | |
|---|---|---|---|
| Ir1-O1 | 1.902 (10) | Ir3-O17 | 1.961 (10)×2 |
| Ir1-O2 | 1.976 (10) | Ir3-O12 | 1.947 (10)×2 |
| Ir1-O3 | 1.940 (10) | Ir3-O13 | 1.957 (10)×2 |
| Ir1-O4 | 1.940 (10) | Ir4-O7 | 1.973 (10) |
| Ir1-O5 | 1.968 (9) | Ir4-O8 | 2.001 (9) |
| Ir1-O6 | 1.973 (10) | Ir4-O9 | 2.002 (10) |
| Ir2-O10 | 1.756 (14)×2 | Ir4-O14 | 1.929 (10) |
| Ir2-O11 | 1.841 (13)×2 | Ir4-O15 | 1.919 (9) |
| | | Ir4-O16 | 1.901 (10) |

$b = 11.876(2)$ Å, $c = 9.969(2)$ Å, $\beta = 93.33°$. The crystal structure data were deposited in Fachinformationszentrum (FIZ) Karlsruhe with Crystal Structure Depot (CSD) number 433206. It represents a new structure type containing four distinct Ir sites: Ir1, Ir3, and Ir4 occupying octahedral sites, and Ir2 residing in an unexpected tetrahedral coordination environment [Fig. 1(a)]. Details of the coordination environment around Ir1 (octahedral) and Ir2 (tetrahedral) are shown in Figs. 1(b) and 1(c), respectively. The anisotropic atomic displacement parameters (ADP) of Ir2 are noticeably prolate, unlike the other Ir ions in octahedral environments, possibly reflecting the unusual coordination environment of Ir2. As shown in Table III, the Ir-O bond lengths in the tetrahedron are 1.756(14) and 1.841(13) Å, considerably shorter than those of the octahedra (1.90–2.00 Å). $Sr_9Ir_3O_{17}$ represents a rare case with 5*d* electrons in a tetrahedral environment.

For transition metal oxides (TMO), the coordination environment of the cations is crucial for virtually all aspects of their physical properties, particularly magnetic and electrical characteristics. The most common coordination environments are octahedral and tetrahedral. Pauling's first rule specifies that the coordination number is determined by the relative sizes of the central cation and its coordinating anions [27]. Accordingly, for relatively small cation-size 3*d* TMO, both tetrahedral and octahedral coordination are common. For 5*d* ions with increasingly large ionic radii, a tetrahedral environment becomes very scarce. Only a few examples have been reported, including $Sc_2W_3O_{12}$ [7], $KReO_4$ [28], $K_2OsO_5$ [29], and $NaOsO_4$ [9], all limited to the $d^0$ or $d^1$ electron configuration with small ionic radii. A recent example with 5*d* ions in the tetrahedral coordination is $KHIrO_4$, but this compound contains hydroxyl groups, which could be better classified as hydroxide instead of oxide [30].

## IV. OXIDATION STATE AND SPIN STATES

The formal oxidation states of Ir in this compound are exceptionally high. Based on its stoichiometry, the average oxidation state for Ir in $Sr_9Ir_3O_{17}$ is +5.33, implying that 2/3 of Ir sites are formally in the oxidation state of +5 and 1/3 in +6. Solid oxides of hexavalent Ir are rare. Examples include $Nd_2K_2IrO_7$ and $Sm_2K_2IrO_7$ [31], both of which were synthesized with a highly oxidizing flux method, and several double perovskites, $A_2MIrO_6$ ($A$ = Ba, Sr, $M$ = Ca, Sr, Mg, Zn) [32], prepared via a high pressure approach. The oxidation state of Ir in $Sr_9Ir_3O_{17}$ was confirmed by x-ray absorption near edge structure (XANES) measurements (Fig. 2).

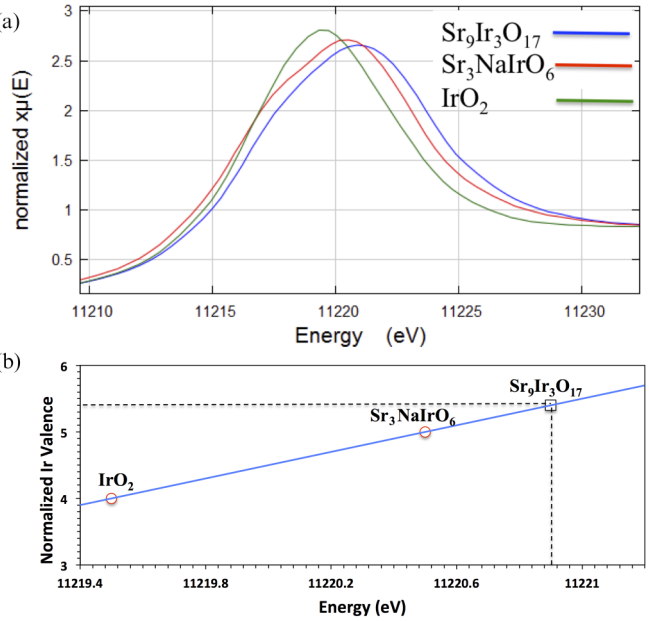


FIG. 2. (a) XANES spectra showing the shift of peak energy for $Sr_9Ir_3O_{17}$ compared with $IrO_2$ and $Sr_3NaIrO_6$ as references. (b) Nominal Ir valence as a function of peak energy. The two open red circles are for $IrO_2$ and $Sr_3NaIrO_6$. The solid blue line is a linear extrapolation based on these two references. The vertical dashed line represents the peak energy measured for $Sr_9Ir_3O_{17}$, which intersects the calibration line at the black open square. The horizontal dashed line establishes the corresponding average oxidation state for Ir, ~5.4.

The XANES spectra show that the peak energy of Ir(V) in $Sr_3NaIrO_6$ is located at ~1 eV higher energy than that of Ir(IV) in the reference compound $IrO_2$. A similar shift was also observed for the formally Ir(VI) compounds $Nd_2K_2IrO_7$ and $Sm_2K_2IrO_7$, for which the peak energy shifted by ~1 eV with respect to a Ir(V) reference oxide [31]. The peak measured for $Sr_9Ir_3O_{17}$ is shifted toward higher energy by approximately 0.4 eV with respect to formally pentavalent $Sr_3NaIrO_6$ [Fig. 2(a)]. Assuming a linear dependence of oxidation state on peak energy [Fig. 2(b)], the XANES assignment of average Ir oxidation state for $Sr_9Ir_3O_{17}$ agrees well with the formal oxidation state of +5.33.

In the tetrahedral Ir2 site, the extended 5*d* orbitals and the notably short Ir-O contacts are expected to result in a higher crystal field splitting than those of typical tetrahedral coordination. DFT calculations were employed to understand the Ir valences as well as the ground state spin configurations. DFT calculations were carried out within the GGA+SOC+$U$ formalism by taking the experimental crystal structure. The projected density of states (DOS) in Fig. 3(a) clearly shows that the four $e$ states are fully occupied, and the sixfold $t_2$ manifold is empty. Thus, the GGA+SOC+$U$ calculations reveal that the tetrahedral Ir2 is in the +5 oxidation state and low spin $e^4t_2{}^0$ configuration. The detailed multiplicities, valence states, electron configurations, etc., of Ir sites are shown in Appendix B (Table V). We would like note that there is no qualitative change in the projected DOS of the tetrahedron even if the calculations are performed without SOC.

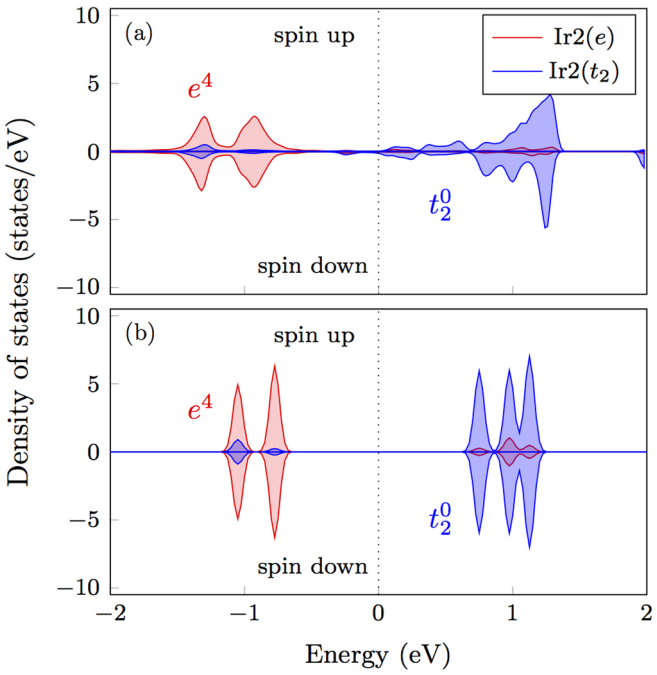


FIG. 3. The calculated projected DOS for Ir2 in bulk $Sr_9Ir_3O_{17}$ (a) and the $[IrO_4]^{3-}$ cluster (b). The upper and lower panel represents the up and down spin states, respectively, and the red and blue lines refer to the $e$ and $t_2$ states, respectively. The chemical potential is set to be zero.

The low spin state of the tetrahedral site can be understood in terms of crystal field splitting. The tetrahedral crystal field splitting $\Delta_{tet}$ is found to be $-2.16$ eV (the center of mass position of the projected DOS for $t_2$ level located at $+1.02$ eV and $e$ level at $-1.14$ eV with respect to the chemical potential at 0 eV), as shown in Fig. 3(b). This crystal field splitting is large for tetrahedral coordination (which is nominally 4/9 of that for the corresponding octahedral configuration); in fact, it is in line with the crystal field splitting scale for octahedral coordination [33]. With this large crystal field, a nonmagnetic low spin configuration ($S = 0$) is stabilized.

This oxidation state and spin configuration are further confirmed by cluster calculations. In the cluster calculations, the charge state of $IrO_4$ was controlled by tuning the background charge while the $IrO_4$ structure is fixed. As shown in Fig. 4, only the electronic structure found for Ir(V), i.e., $(IrO_4)^{3-}$, is in good agreement with the full periodic calculation result, while those of states (PDOS) for $[IrO_4]^{2-}$ and $[IrO_4]^{4-}$ disagree with the periodic bulk calculations (Fig. 4). The calculated Mulliken charge is 7.57, 7.79, and 7.96 for $[IrO_4]^{2-}$, $[IrO_4]^{3-}$, and $[IrO_4]^{4-}$ cluster, respectively while the periodic calculation gives 7.85. Thus, the cluster calculation results, consistent with the bulk result, further confirm the valence assignment.

## V. MAGNETIC DATA

Magnetic data were collected to further probe the valences and electron configuration. The magnetic susceptibility of $Sr_9Ir_3O_{17}$, which was corrected for diamagnetic contributions

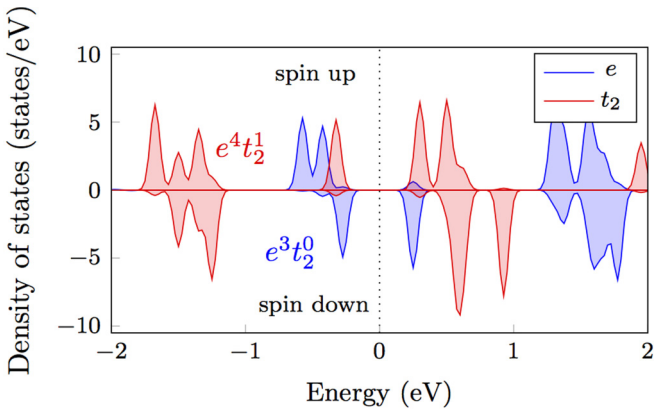


FIG. 4. PDOS of Ir-5$d$ orbitals. The result of $[IrO_4]^{2-}$ ($d^3$) and $[IrO_4]^{4-}$ ($d^5$) is presented in blue and red, respectively.

of core electrons [34], shows an antiferromagnetic ordering at 11 K (Fig. 5), and follows a Curie-Weiss behavior in the paramagnetic regime ($T > 11$ K). For ease of assigning spin states to the four Ir sites in the crystal, we have taken the formula unit (fu) as $Sr_{36}Ir_{12}O_{68}$. A linear fit to $1/\chi$ yields a Curie constant of 9.90 emu K/(mol Oe), which equates to an effective moment of 8.90 $\mu_B$/fu, and a Weiss temperature of $-54.6$ K. Using a simplified, local model to provide insight into the spin states, we have attempted to assign site-specific oxidation states and spin configurations based on these susceptibility data by decomposing the structure into local moments that sum in quadrature to the full moment of the compound (i.e., $p_{\text{eff}}^2 = \sum_i p_i^2$, where $p_i^2$ is the local effective moment on site $i$). We begin in a limit with no SOC, i.e., assuming a spin-only model, idealized octahedra and tetrahedral geometries, $g = 2$, and formula unit $Sr_{36}Ir_{12}O_{68}$. No consideration of Ir-O hybridization (i.e., O-localized spin)

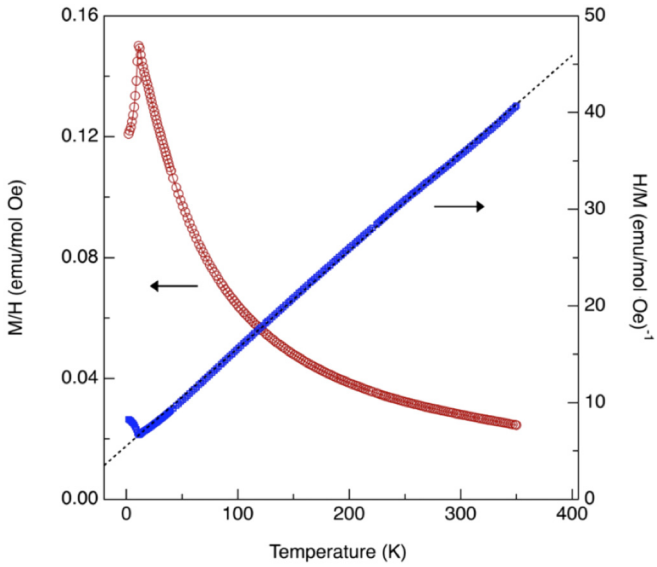


FIG. 5. Magnetic susceptibility and inverse magnetic susceptibility of $Sr_{36}Ir_{12}O_{68}$ versus temperature. Data were corrected for diamagnetic contributions of core electrons. The linear fitting demonstrates the title compound follows Curie-Weiss behavior.

is taken into account. Under this simplified model, the +5 octahedral Ir1 and Ir3 have four electrons in the low spin state, leaving two unpaired electrons in 5*d* orbitals. The spin-only effective moment of this site, $p_{\rm eff}(O_h, 5+)^2 = 8\,{\mu_{\rm B}}^2$. Another octahedral site of +6 Ir4 has three unpaired 5*d* electrons, $p_{\rm eff}(O_h, 6+)^2 = 15\,{\mu_{\rm B}}^2$. For the tetrahedral Ir2, the +5 oxidation state and a low spin configuration gives no unpaired electrons, i.e., $e^4{t_2}^0$, $p_{\rm eff}(T_d, 5+)^2 = 0$. With a formula unit $Sr_{36}Ir_{12}O_{68}$, and the multiplicities of the crystallographic sites for Ir1:Ir2:Ir3:Ir4 in the ratio 4:2:2:4, ${p_{\rm eff}}^2/{\rm fu} = 32\,{\mu_{\rm B}}^2 + 0\,{\mu_{\rm B}}^2 + 16\,{\mu_{\rm B}}^2 + 60\,{\mu_{\rm B}}^2 = 108\,{\mu_{\rm B}}^2$ and hence an expected spin-only moment of $10.39\,\mu_{\rm B}$/fu, which is considerably larger than that obtained experimentally. This discrepancy would be even more significant if we were to choose to assign Ir2 to a high spin state, for which the calculated moment would be $12.49\,\mu_{\rm B}$/fu.

An alternative scenario is to invoke a strong spin-orbit coupling case, yet for which the crystal field splitting $\Delta$ is large compared to SOC so as to isolate the description to the $t_{2g}$-derived states. This yields for the octahedral sites (Ir1, Ir3, Ir4) a $J_{\rm eff} = 3/2$ quartet and $J_{\rm eff} = 1/2$ doublet formed out of the sixfold $t_{2g}$ states [26]. In this picture, the 5*d* [4] $Ir^{5+}$ ion on the Ir1 and Ir3 sites corresponds to a filled $J_{\rm eff} = 3/2$ manifold nonmagnetic state, and a tetrahedral $d^4$ Ir2 remains closed shell and nonmagnetic as well. That leaves a hexavalent Ir4 in octahedral coordination as the only potential magnetic ion. Following the discussion by Matsuura and Miyake [37], for octahedral 5*d* [3] ions in the limit of large SOC, $M = 0$ as well. Experimentally, $Sr_9Ir_3O_{17}$ is magnetic, implying that Ir4 must lie in a regime of intermediate strength SOC, with an effective moment suppressed below the spin-only value of $p_{\rm eff} = 3.87\,\mu_{\rm B}$/Ir or $7.75\,\mu_{\rm B}$/fu.

It is clear that simplified, local models such as these are inadequate to describe the magnetic states of $Sr_3Ir_9O_{17}$. For instance, significant covalency expected to accompany the high formal oxidation state of Ir in $Sr_9Ir_3O_{17}$ is ignored and may lead to nonzero spin density on the coordinated O sites.

The magnetic behavior can be better understood within our band structure calculations. We found that spin and/or magnetic moments are distributed across the octahedral or tetrahedral coordination polyhedra that comprise the structure rather than being localized at atomic Ir sites. Thus, the influence of hybridization is naturally included in the calculation. Due to the large intercluster distances separating $IrO_6$ and/or $IrO_4$, this local cluster moment around the Ir sites is always well defined. Assuming that $J$ is a good quantum number, the *g*-factor $g_{\rm J} = |\vec{\mu}|/|\vec{J}| = |\vec{L} + 2\vec{S}|/|\vec{L} + \vec{S}|$. The estimated $g_{\rm J}$ value is 1.70, 1.66, 1.59, and 1.96 for Ir1, Ir2, Ir3, and Ir4, respectively. The effective moment is given by $\mu_{\rm eff}^2 = g_{\rm J}^2\mu_{\rm B}^2 J(J+1) \approx g_{\rm J}^2\mu_{\rm B}^2 J_z(J_z+1)$. In the last expression, the moments are regarded as being fully polarized so that $J = J_z$. From our GGA+SOC+$U$ calculations, $J_z$ and $\mu_{\rm eff}$ for Ir1, Ir2, Ir3, I4 are found to be 1.26, 0.08, 1.09, 1.31 and 2.87, 0.49, 2.41, 3.41, respectively. These values for octahedral sites with $d^3$ (Ir4 site) and $d^4$ Ir (Ir1, Ir3 sites) ions reflect the reasonable electronic structure considering the noncubic crystal field splitting (∼0.12–0.26 eV) within the $t_{2g}$ manifolds and the SOC (∼0.4 eV) of Ir-5*d* orbitals [26,35]. The $\mu_{\rm eff}$ values are close to those expected from spin-only considerations (2.83 and $3.87\,\mu_{\rm B}$), implying that $J_{\rm eff} = 3/2$ is not a good basis despite the sizable SOC. As expected, Ir2 makes a negligible contribution $\mu_{\rm eff} \sim 0\,\mu_{\rm B}$. Finally, from the formula unit of $Sr_{36}Ir_{12}O_{68}$, by summing the individual cluster effective moments in quadrature weighted by their populations (Ir1:Ir2:Ir3:Ir4 = 4:2:2:4), the magnetic moment was calculated to be $9.56\,\mu_{\rm B}$/fu (the contribution from orbital moment is $1.54\,\mu_{\rm B}$/fu). The value is in reasonable agreement with the measured effective moment of $8.90\,\mu_{\rm B}$/fu, further corroborating the electronic configuration of $e^4t_2^0$ for Ir2.

The calculation reveals a considerable hybridization between Ir-5*d* and O-2*p*, perhaps not unexpected for the high formal oxidation states of Ir in $Sr_9Ir_3O_{17}$. For example, if we only consider the Mulliken charge on Ir sites, the effective moment becomes considerably smaller, $6.39\,\mu_{\rm B}$/fu. We also found O ions have non-negligible moments $\sim 0.14-0.67\,\mu_{\rm B}$. The DFT results also emphasize the important role of SOC in the description of magnetism. Without SOC, the effective moment is $10.64\,\mu_{\rm B}$/fu, which is larger than the observed moment and is indeed closer to the simple estimation of $10.39\,\mu_{\rm B}$/fu based on the nominal charge and spin assignment above.

## VI. CRYSTAL CHEMISTRY CONSIDERATIONS

The particularly short bond lengths for the tetrahedral site provide further evidence for the low spin state. The Ir-O bond lengths of 1.756(14) and 1.841(13) Å for the tetrahedral Ir2 sites are conspicuously short. The ionic radii for $O^{2-}$ is 1.35 Å [36]. Thus, given the Ir-O bond length of 1.756 Å, the ionic radius of this Ir cannot be larger than 0.40 Å. With such a small ionic radius, the Ir site can only be in a low spin configuration.

Moreover, valuable information can be obtained by comparing the bond lengths with the W(VI), Re(VII), and Os(VIII) oxides. $Sc_2W_3O_{12}$ [7], $KReO_4$ [28], and $K_2OsO_5$ [29] represent the few 5*d* transition metal oxides with tetrahedral coordination. The bond lengths of W–O, Re–O, and Os–O are 1.76–1.77 Å, 1.72 Å, and 1.74–1.83 Å in these compounds, respectively. Note that these short bond lengths are consistent with their electronic configuration of an empty shell. In $Sr_9Ir_3O_{17}$, the bond lengths in the tetrahedral are 1.756(14) and 1.841(13) Å, which are very close to the tetrahedral W–O, Re–O, and Os–O bond lengths with empty shell. It is known that cations with an empty shell tend to have smaller ionic radii [36,38], and consequently short bond lengths. The fact that the Ir-O in the tetrahedral site of $Sr_9Ir_3O_{17}$ is close to those of the 5*d* cations with empty shell in the tetrahedral indicates that Ir is in $e^4t_2^0$ configuration, rather than a high spin configuration.

Tetrahedral coordination in oxides is uniformly found in high-spin configuration due to the modest crystal field stabilization energy (CFSE) vis-à-vis the cost in lost exchange energy from pairing energy of the spins. Since 5*d* orbitals are more extended than their 3*d* and 4*d* counterparts, stronger overlaps with the coordinating ligands are expected, leading to a larger crystal field.

$Sr_9Ir_3O_{17}$ appears to realize the unexpected tetrahedral low spin state. Previously, the only reported 5*d* oxide with a finite *d* electron count is $AOsO_4$($A$ = Na, K) [9]. With a

$d^1$ configuration, the spin state of the cation is irrelevant. In fact, to the best of our knowledge, $Sr_9Ir_3O_{17}$ is the only 5*d* oxide reported with tetrahedral coordination having more than 2 electrons, for which spin state can be possibly tuned. Moreover, with four 5*d* electrons in tetrahedral coordination, Ir(V) gains maximal CFSE by adopting the low spin state in a completely filled $e^4$ orbital subshell. Thus, the extended 5*d* orbital, small cation size, and $e^4t_2^0$ configuration provides a unique platform for realizing this exceedingly rare low spin state in the tetrahedral oxide environment. The extended orbital can also have profound effect on other 5*d* cations, such as Os(IV), and novel ground state may occur in proper coupling with other characteristics of the specific materials. We note that $KHIrO_4$ with a hydrogeniridate(VI) anion and a $d^3$ electron count was recently reported [30]. The spin state of Ir(VI) in this compound, which is better classified as a hydroxide, was not reported, but may well also be low spin based on our findings here.

## VII. CONCLUSIONS

An extremely unusual low spin state in tetrahedral coordination is realized in $Sr_9Ir_3O_{17}$. This electronic configuration is proved by GGA+SOC+*U* formalism, cluster calculation, magnetic data, as well as bond lengths. A confluence of electronic factors—extended 5*d* orbitals, short bond lengths, and a half-filled subshell for maximal CFSE—converge in $Sr_9Ir_3O_{17}$ to realize this rare spin state. The realization of the low spin state in tetrahedral coordination may provide a novel platform for spin state manipulation in solids.

## ACKNOWLEDGMENTS

Work at Argonne National Laboratory (crystal growth, structural and magnetic measurements) was supported by the US Department of Energy Office of Science, Basic Energy Sciences, Materials Science and Engineering Division. Q.Z. was supported by National Natural Science Foundation of China (11404358). J.H.S. and M.J.H. were supported by Basic Science Research Program through the National Research Foundation of Korea (NRF) funded by the Ministry of Education (2018R1A2B2005204) and Creative Materials Discovery Program through the NRF funded by Ministry of Science and ICT (2018M3D1A1058754). Computational resources were provided by KISTI (KSC2015-C2-011). This work was supported by the National Key Project for Basic Research of China (2017YFA0303403), Shanghai Science and Technology Innovation Action Plan (No. 17JC1402500). Q.Z. was supported by the startup funds from Washington State University. This research used resources of the Advanced Photon Source, an Office of Science User Facility operated for the US Department of Energy (DOE) Office of Science by Argonne National Laboratory, and was supported by the U.S. DOE under Contract No. DE-AC02-06CH11357. Helpful discussions with Dr. Mike H. Whangbo, Dr. Xiangang Wan, and Dr. Gang Mu are acknowledged.

The authors declare no conflict of interest.

## APPENDIX A: ANISOTROPIC DISPLACEMENT PARAMETERS

The anisotropic displacement parameters are listed in Table IV.

TABLE IV. Anisotropic displacement parameters ($Å^2 \times 10^3$) for $Sr_9Ir_3O_{17}$ at 100 K with estimated standard deviations in parentheses.[a]

| | *U* [11] | *U* [22] | *U* [33] | *U* [12] | *U* [13] | *U* [23] |
|---|---|---|---|---|---|---|
| Ir1 | 0.0228 (4) | 0.0222 (4) | 0.0217 (3) | 0.0001 (2) | 0.0010 (3) | 0.0000 (2) |
| Ir2 | 0.0312 (6) | 0.0279 (5) | 0.0807 (8) | 0.000 | -0.0059 (5) | 0.000 |
| Ir3 | 0.0220 (5) | 0.0220 (5) | 0.0223 (4) | 0.000 | 0.0009 (3) | 0.000 |
| Ir4 | 0.0235 (4) | 0.0235 (4) | 0.0226 (3) | 0.0006 (2) | 0.0010 (3) | 0.0000 (2) |
| Sr1 | 0.0236 (7) | 0.0250 (7) | 0.0265 (7) | −0.0009 (6) | 0.0010 (6) | 0.0022 (6) |
| Sr2 | 0.0303 (8) | 0.0273 (7) | 0.0271 (7) | −0.0039 (6) | 0.0023 (6) | −0.0009 (6) |
| Sr3 | 0.0405 (9) | 0.0364 (9) | 0.0261 (8) | −0.0152 (7) | 0.0043 (7) | −0.0013 (6) |
| Sr4 | 0.0274 (8) | 0.0281 (8) | 0.0250 (7) | 0.0051 (6) | −0.0002 (6) | −0.0029 (6) |
| Sr5 | 0.0250 (7) | 0.0231 (7) | 0.0251 (7) | 0.0012 (6) | 0.0029 (6) | −0.0006 (5) |
| Sr6 | 0.0245 (7) | 0.0235 (7) | 0.0254 (7) | 0.0024 (6) | 0.0020 (5) | 0.0013 (5) |
| Sr7 | 0.0234 (7) | 0.0293 (8) | 0.0276 (7) | 0.0005 (6) | 0.0024 (6) | 0.0016 (6) |
| Sr8 | 0.0251 (8) | 0.0247 (7) | 0.0279 (7) | −0.0015 (6) | 0.0035 (6) | −0.0029 (6) |
| Sr9 | 0.0229 (8) | 0.0289 (8) | 0.0394 (8) | −0.0009 (6) | 0.0002 (6) | 0.0107 (6) |
| O1 | 0.026 (6) | 0.022 (5) | 0.025 (5) | 0.000 (4) | −0.005 (4) | −0.002 (4) |
| O2 | 0.023 (5) | 0.029 (6) | 0.033 (6) | −0.001 (4) | 0.006 (4) | −0.007 (5) |
| O3 | 0.037 (6) | 0.019 (5) | 0.030 (6) | −0.007 (4) | −0.003 (5) | 0.003 (4) |
| O4 | 0.023 (5) | 0.027 (6) | 0.021 (5) | −0.003 (4) | −0.006 (4) | −0.003 (4) |
| O5 | 0.031 (6) | 0.023 (5) | 0.021 (5) | −0.006 (4) | 0.004 (4) | 0.002 (4) |
| O6 | 0.037 (6) | 0.034 (6) | 0.020 (5) | 0.014 (5) | 0.000 (4) | −0.004 (4) |
| O7 | 0.035 (6) | 0.030 (6) | 0.027 (5) | 0.003 (5) | 0.005 (5) | 0.008 (4) |
| O8 | 0.018 (5) | 0.033 (6) | 0.027 (5) | 0.012 (4) | 0.000 (4) | −0.007 (4) |
| O9 | 0.031 (6) | 0.020 (5) | 0.032 (6) | 0.000 (4) | −0.004 (5) | −0.001 (4) |

TABLE IV. (*Continued.*)

| | *U* [11] | *U* [22] | *U* [33] | *U* [12] | *U* [13] | *U* [23] |
|---|---|---|---|---|---|---|
| O10 | 0.050 (5) | 0.053 (5) | 0.067 (5) | -0.001 (4) | 0.002 (4) | −0.002 (4) |
| O11 | 0.053 (5) | 0.065 (5) | 0.047 (5) | −0.012 (4) | 0.009 (4) | −0.010 (4) |
| O12 | 0.024 (5) | 0.019 (5) | 0.027 (5) | −0.006 (4) | 0.004 (4) | −0.005 (4) |
| O13 | 0.030 (6) | 0.026 (5) | 0.024 (5) | 0.008 (4) | −0.001 (4) | −0.002 (4) |
| O14 | 0.031 (6) | 0.033 (6) | 0.023 (5) | 0.009 (5) | 0.001 (4) | 0.001 (4) |
| O15 | 0.038 (6) | 0.024 (5) | 0.022 (5) | 0.001 (5) | −0.004 (4) | 0.004 (4) |
| O16 | 0.025 (6) | 0.027 (5) | 0.026 (5) | −0.003 (4) | 0.005 (4) | 0.001 (4) |
| O17 | 0.028 (6) | 0.024 (5) | 0.021 (5) | 0.002 (4) | −0.002 (4) | −0.005 (4) |

[a]The anisotropic displacement factor exponent takes the form $-2\pi^2[h^2a^{*2}U_{11} + \cdots + 2hka^*b^*U_{12}]$.

## APPENDIX B: THE MULTIPLICITY AND CHARGE STATE OF IR SITES

The charge and electronic states of different Ir sites are shown in Table V.

TABLE V. The multiplicities of the crystallographic sites, local environments, oxidation states, Mulliken populations, and electron configurations for Ir.

| | Multiplicity | Local environment | Oxidation state[a] | Mulliken population | Electron configuration | Effective moment ($\mu_B$)[b] |
|---|---|---|---|---|---|---|
| Ir1 | 4 | Octahedra | +5 ($d^4$) | 7.15 | $t_{2g}^4e_g^0$ | 2.87 |
| Ir2 | 2 | Tetrahedra | +5 ($d^4$) | 7.39 | $e^4t_2^0$ | 0.49 |
| Ir3 | 2 | Octahedra | +5 ($d^4$) | 7.21 | $t_{2g}^4e_g^0$ | 2.41 |
| Ir4 | 4 | Octahedra | +6 ($d^3$) | 7.02 | $t_{2g}^3e_g^0$ | 3.41 |

[a]Oxidation state of Ir1 is assigned to the most probable formal charge based on the stoichiometry.
[b]Based on GGA+SOC+*U* calculations, see text for details.


[1] J.-F. Lin, V. V. Struzhkin, S. D. Jacobsen, M. Y. Hu, P. Chow, J. Kung, H. Liu, H. Mao, and R. J. Hemley, Nature (London) **436**, 377 (2005).
[2] J. B. Wittenberg, B. A. Wittenberg, J. Peisach, and W. E. Blumberg, Proc. Natl. Acad. Sci. USA **67**, 1846 (1970).
[3] J. A. Real, A. B. Gaspar, and M. C. Muñoz, Dalton Trans. 2062 (2005).
[4] T. Vogt, P. M. Woodward, P. Karen, B. A. Hunter, P. Henning, and A. R. Moodenbaugh, Phys. Rev. Lett. **84**, 2969 (2000).
[5] Y. Moritomo, T. Akimoto, M. Takeo, A. Machida, E. Nishibori, M. Takata, M. Sakata, K. Ohoyama, and A. Nakamura, Phys. Rev. B **61**, R13325 (2000).
[6] R. Mahendiran and A. K. Raychaudhuri, Phys. Rev. B **54**, 16044 (1996).
[7] S. C. Abrahams and J. L. Bernstei, J. Chem. Phys. **45**, 2745 (1966).
[8] J. C. Morrow, Acta Cryst. **13**, 443 (1960).
[9] W. Levason, M. Tajik, and M. Webster, J. Chem. Soc. Dalton Trans. 1735 (1985).
[10] G. J. Wang, M. F. Zhou, J. T. Goettel, G. J. Schrobilgen, J. Su, J. Li, T. Schloder, and S. Riedel, Nature (London) **514**, 475 (2014).
[11] T. Reier, M. Oezaslan, and P. Strasser, ACS Catal. **2**, 1765 (2012).
[12] P. Lettenmeier, L. Wang, U. Golla-Schindler, P. Gazdzicki, N. A. Cañas, M. Handl, R. Hiesgen, S. S. Hosseiny, A. S. Gago, and K. A. Friedrich, Angew. Chem. Int. Ed. **55**, 742 (2016).
[13] G. M. Sheldrick, Acta Cryst. A **64**, 112 (2008).
[14] B. Ravel and M. Newville, J. Synchrotron Radiat. **12**, 537 (2005).
[15] I. D. Brown and D. Altermatt, Acta Cryst. B **41**, 244 (1985).
[16] N. E. Brese and M. Okeeffe, Acta Cryst. B **47**, 192 (1991).
[17] T. Ozaki, Phys. Rev. B **67**, 155108 (2003).
[18] http://www.openmx-square.org.
[19] J. P. Perdew, K. Burke, and M. Ernzerhof, Phys. Rev. Lett. **77**, 3865 (1996).
[20] A. H. MacDonald, J. Phys. C: Solid State Phys. **16**, 3869 (1983).
[21] M. J. Han, T. Ozaki, and J. Yu, Phys. Rev. B **73**, 045110 (2006).
[22] S. L. Dudarev, G. A. Botton, S. Y. Savrasov, C. J. Humphreys, and A. P. Sutton, Phys. Rev. B **57**, 1505 (1998).
[23] K. H. Kim, H. S. Kim, and M. J. Han, J. Phys.: Condens. Matter **26**, 185501 (2014).
[24] J.-H. Sim, H. Yoon, S. H. Park, and M. J. Han, Phys. Rev. B **94**, 115149 (2016).
[25] H. S. Kim, J. Im, M. J. Han, and H. Jin, Nat. Commun. **5**, 3988 (2014).
[26] B. J. Kim, H. Jin, S. J. Moon, J. Y. Kim, B. G. Park, C. S. Leem, J. Yu, T. W. Noh, C. Kim, S. J. Oh, J. H. Park, V. Durairaj, G. Cao, and E. Rotenberg, Phys. Rev. Lett. **101**, 076402 (2008).
[27] L. Pauling, J. Am. Chem. Soc. **51**, 1010 (1929).
[28] R. H. Plovnick and G. E. Schmidt, J. Cryst. Growth **8**, 309 (1971).
[29] K. M. Mogare, W. Klein, and M. Jansen, Z. Anorg. Und Allg. Chem. **631**, 468 (2005).

[30] M. T. Weller and R. Galati, Inorg. Chem. **53**, 5405 (2014).
[31] S. J. Mugavero, M. D. Smith, W. S. Yoon, and H. C. zur Loye, Angew. Chem. Int. Ed. **48**, 215 (2009).
[32] D. Y. Jung and G. Demazeau, J. Solid State Chem. **115**, 447 (1995).
[33] K. Kushida and K. Kuriyama, Appl. Phys. Lett. **77**, 4154 (2000).
[34] P. Selwood, *Magnetochemistry*, 2nd ed. (Interscience, New York, 1956).
[35] G. Cao, T. F. Qi, L. Li, J. Terzic, S. J. Yuan, L. E. DeLong, G. Murthy, and R. K. Kaul, Phys. Rev. Lett. **112**, 056402 (2014).
[36] R. D. Shannon, Acta Cryst. A **32**, 751 (1976).
[37] H. Matsuura and K. Miyake, J. Phys. Soc. Jpn. **82**, 073703 (2013).
[38] F. A. Cotton, G. Wilkinson, C. Murrillo, and M. Bochmann, *Advanced Inorganic Chemistry*, 6th ed. (John Wiley & Sons, New York, 1999).